Solar Phys (2007) 240: 241–252
DOI 10.1007/s11207-007-0263-1

Analysis of RHESSI Flares Using a Radio Astronomical Technique

E.J. Schmahl · R.L. Pernak · G.J. Hurford · J. Lee · S. Bong

Received: 5 June 2006 / Accepted: 29 December 2006 /
Published online: 2 March 2007

Abstract We have used Ramaty High Energy Solar Spectroscopic Imager (RHESSI) modulation profiles in the 25 – 300 keV range to construct high-fidelity visibilities of 25 flares having at least two components. These hard X-ray visibilities, which are mathematically identical to the visibilities of radio imaging, were input to software developed for mapping solar flares in the microwave domain using the Maximum Entropy Method (MEM). We compared and contrasted the MEM maps with Clean and Pixon maps made with RHESSI software. In particular, we assessed the reliability of the maps and their morphologies for future investigations of the symmetry of bipolar electron beaming in the sample set.

Keywords Sun: X-rays · Sun: flares · Instruments · Image processing · Numerical methods

E.J. Schmahl
Astronomy Department, University of Maryland, College Park, MD 20742, USA

E.J. Schmahl · R.L. Pernak (✉)
Laboratory for Solar and Space Physics, NASA Goddard Space Flight Center, Greenbelt, MD 20771, USA
e-mail: pernak@lssp-mail.gsfc.nasa.gov

R.L. Pernak
Institute for Astrophysics and Computational Sciences, The Catholic University of America, Washington, DC 20064, USA

G.J. Hurford
Space Sciences Laboratory, University of California, Berkeley, CA 94720, USA

J. Lee
Center for Solar and Terrestrial Research, New Jersey Institute of Technology, Newark, NJ 07102, USA

S. Bong
Korean Astronomy and Space Science Institute, Daejeon, 305-348, Korea

1. Introduction

Mapping with visibilities has a rich history in radio astronomy. Visibilities themselves are samples of the Fourier transform of the source in the image plane. Given dense sampling of the u, v plane (with u and v the coordinates of the Fourier plane), the inverse Fourier transform yields a map. Since the u, v sampling is not usually dense, and is often quite sparse, the map so produced is called the "dirty map." Various methods have been devised to remove the sidelobes produced by sparse sampling in the dirty map and we selected the Maximum Entropy Method (MEM) for this study.

The Ramaty High Energy Solar Spectroscopic Imager (RHESSI) has been observing flares since February 2002 (Lin *et al.*, 2002). RHESSI is the first HXR imager to use Fourier-based methods with high spectral ($\sim$1 keV) energy resolution in the 3 keV to 17 MeV range, although previous lower-resolution Fourier-based imagers — Hinotori and Yohkoh/HXT — have provided abundant proof of principle of this method of imaging. The amplitudes and phases of RHESSI's modulation profiles are analogous to the amplitudes and phases derived from radio interferometers (Hurford *et al.*, 2002). After calibration, these amplitudes and phases become device-independent (Hurford, Schmahl, and Schwartz, 2005) and are precisely equivalent to radio visibilities. Other methods of HXR imaging have been developed for RHESSI (Schwartz *et al.*, 2002). Among them are Back projection, Clean, and Pixon, and these can provide validation and testing of the MEM images.

1.1. Existing Software

Software that has already been used in RHESSI data analysis include Back projection, Clean, Pixon and two Maximum Entropy routines. These mapping methods have previously been evaluated for photometric accuracy by Aschwanden *et al.* (2004). All appear to have fundamental flaws, but comparison of all the maps produced by the different algorithms gives a good picture as to what a "true map" might be.

Back projection maps are analogous to Fourier transforms of observed visibilities in radio astronomy (Hurford *et al.*, 2002). Back projection is RHESSI's simplest image reconstruction algorithm. It is essentially a sum of probability maps — RHESSI detectors by themselves cannot determine where a photon actually comes from, so position of the source can only be based on probability distributions derived from the subcollimator geometries and aspect system solutions. The probability maps are weighted with the modulated intensity profiles. Given at least half a rotation of data, Back projection can produce a map. Though the addition of probability maps is straightforward and efficient, an undesired by-product of the process is the presence of "sidelobes," which appear as ringlets around the source positions.

Clean is another radio-based concept. Any extended source is treated as a superposition of point sources, which are extracted from the "dirty map" then convolved with the Clean beam (a Gaussian source reflecting the resolution of the subcollimators used). Here, the dirty map is the Back projection map. The process involves selecting the brightest pixels, subtracting out a fraction of the maximum multiplied by the point spread function, and repeating this until a number of iterations is reached or the maximum is negative. Clean is reliable because it produces what Back projection does but removes the sidelobes. However, the algorithm is not always a dependable method of determining source flux because too much of the map flux appears in the background.

The Pixon method, in contrast, is widely considered the most photometrically dependable imaging reconstruction algorithm. It produces what is supposed to be the simplest model for

the image that is consistent with the data (Puetter, 1995). The model incorporates groups of pixels called "pixons" that are iteratively selected until the resultant modulation profile matches the data (*i.e.*, has a small χ^2). The tradeoff one must accept when relying on Pixon's flux reliability is its lack of efficiency — Pixon is one to two magnitudes slower than any other imaging algorithm.

The Maximum Entropy Method (MEM) is described in more detail in the following, but for now it should be noted that previous MEM programs used by RHESSI, MEM_VIS, and MEM_SATO have not been successful. MEM_VIS, like MEM_NJIT, is a visibility-based MEM. Its flaw is that maps produced by multiple rotations get gradually worse after one rotation. MEM_SATO is a fixed-point method similar to the MEM procedure used by Yohkoh/HXT (Sato, Kosugi, and Makishima, 1999). It does not consistently converge on a good map, and it requires a small field of view.

1.2. RHESSI Visibilities

Each amplitude (A_j) and phase (ϕ_j) computed from RHESSI modulation profiles are combined into visibilities (V_j) in the standard way:

$$V_j = A_j \exp(i\phi_j). \tag{1}$$

The result is an array of complex values, each defined at a point in the Fourier plane.

Since RHESSI is a rotating modulation collimator (RMC) with a set of nine grid pairs, each with pitches at multiples of $\sqrt{3}$, the Fourier coordinates (u_j, v_j) lie on nine circles whose radii are multiples of $1/\sqrt{3}$ in the Fourier plane. Each circle has a radius $|k_i| = \sqrt{u_i^2 + v_i^2}$ given by the reciprocal of the angular pitch of the ith subcollimator (Hurford *et al.*, 2002):

$$k_i = \frac{1}{p_1 * 3^{(i-1)/2}} \text{ arcsec}^{-1}, \quad i = 1, 2, \ldots, 9. \tag{2}$$

The quantity p_1 in this equation is the angular pitch of the finest subcollimator, which provides modulation for spatial scales of $2.3''$. The smallest k_i for the coarsest subcollimator 9, provides an amplitude closest to the total flux. For the best (u, v) coverage, one must use as many of the (u, v) circles as possible, consistent with the minimization of "over-resolution" and noise and avoidance of RHESSI's spin axis (Hurford *et al.*, 2002, Section 4.1). Typically, this means using circles 3 – 8, although some compact flares permit the use of circles 2 – 8, and some extended sources require restricting the range to 4 – 8.

1.3. The Maximum Entropy Method

MEM imaging was first developed by Jaynes (1957, 1968) and has been widely used in a variety of fields. The basis of the method is to maximize the information entropy H while minimizing a measure of the goodness of fit (usually χ^2) and maintaining the correct value of the flux. In practice, following Cornwell and Evans (1985), one maximizes the objective function:

$$J = H - \alpha\chi^2 - \beta F \tag{3}$$

over the parameter space of all possible images. Here, α and β are Lagrange multipliers, χ^2 is the statistical measure of goodness of fit to the data, and F is the flux, *i.e.*, the sum of pixel brightnesses. Differentiating Equation (3) with respect to pixel brightnesses and setting that gradient equal to zero gives

$$\nabla J = \nabla H - \alpha\nabla\chi^2 - \beta = 0. \tag{4}$$

1.4. MEM_NJIT

Bong *et al.* (2005, 2006) have developed a MEM program following these principles that maps Owens Valley Solar Array (OVSA) data. In its original form, it is a 3-D MEM, using not only u, v but frequency ν as a third independent coordinate. The solar group at New Jersey Institute of Technology (NJIT) has provided the 2-D (single-frequency) MEM version to the RHESSI team and dubbed it MEM_NJIT.

The program requires user input of visibilities and their uncertainties, and u and v values — all are generated from RHESSI data by RHESSI visibility software and visibility data form a structure. The structure contains all the required mapping data as well as subcollimator indices, energy ranges, time intervals, estimated fluxes, χ^2 measurements, and map centers. MEM_NJIT uses the flux of the map as computed from the visibility amplitudes.

2. Observations

We have selected 25 well-resolved double-component flares from the more than 20,000 events in the RHESSI dataset. Flare times, detectors, and energies are provided in Table 1.

Table 1 Data for the 25 flares used in this study. Flare numbers correspond to the numbers in the lower right-hand corner in Figures 1, 2, and 3.

Flare number	Date	Time interval	Detectors	Energy (keV)
1	20 Feb 2002	11:06:00 – 11:06:36	345678	25.0 – 50.0
2	23 Jul 2002	00:41:00 – 00:44:40	45678	50.0 – 100.0
3	20 Aug 2002	01:44:20 – 01:45:20	345678	25.0 – 50.0
4	8 Sep 2002	01:42:20 – 01:43:20	2345678	25.0 – 50.0
5	20 Sep 2002	09:26:08 – 09:27:08	2345678	25.0 – 50.0
6	9 Nov 2002	13:21:04 – 13:22:04	45678	25.0 – 50.0
7	18 Mar 2003	12:14:00 – 12:15:00	2345678	50.0 – 100.0
8	2 Jun 2003	00:13:28 – 00:14:28	345678	25.0 – 50.0
9	9 Jun 2003	11:24:12 – 11:25:12	2345678	50.0 – 100.0
10	10 Jun 2003	11:06:16 – 11:07:16	45678	25.0 – 50.0
11	19 Oct 2003	16:43:04 – 16:44:04	45678	25.0 – 50.0
12	24 Oct 2003	02:55:52 – 02:56:52	45678	25.0 – 50.0
13	19 Nov 2003	03:59:28 – 04:00:28	2345678	25.0 – 50.0
14	30 Oct 2004	16:23:48 – 16:24:48	45678	25.0 – 50.0
15	31 Oct 2004	02:23:04 – 02:24:04	345678	25.0 – 50.0
16	31 Oct 2004	05:31:20 – 05:32:20	45678	25.0 – 50.0
17	6 Nov 2004	00:30:24 – 00:31:24	45678	50.0 – 100.0
18	1 Dec 2004	07:09:56 – 07:11:56	45678	25.0 – 50.0
19	15 Jan 2005	22:42:46 – 22:44:20	45678	25.0 – 50.0
20	20 Jan 2005	06:42:10 – 06:43:30	45678	100.0 – 300.0
21	13 Jul 2005	14:21:00 – 14:24:00	45678	50.0 – 100.0
22	30 Jul 2005	06:30:30 – 06:33:30	45678	50.0 – 100.0
23	22 Aug 2005	17:04:16 – 17:05:16	345678	25.0 – 50.0
24	10 Sep 2005	21:32:00 – 21:34:00	345678	50.0 – 100.0
25	17 Sep 2005	06:02:10 – 06:02:30	345678	25.0 – 50.0

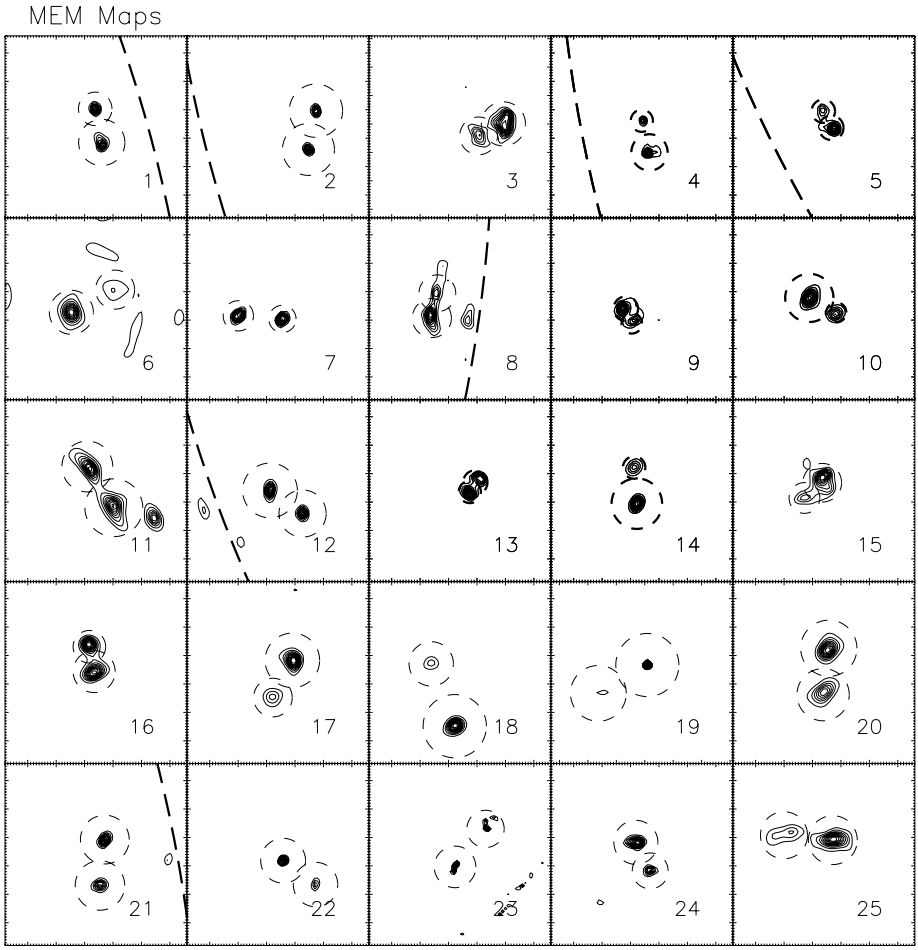

Figure 1 MEM_NJIT maps of 25 double-component flares in the 25 – 50 keV band. Contour levels are 10, 20, 30, 40, 50, 60, 70, 80, 90, and 100% of the maximum flux. The spatial scale is 2 arcsec pixel^{-1} and the field of view is 128 × 128 arcsec. The dashed circles represent regions where fluxes were calculated.

Our goal is to validate the MEM imaging and compare MEM with other imaging methods (Clean and Pixons). A similar study was conducted on the photometric accuracy of RHESSI imaging algorithms, and our results are generally in agreement (Aschwanden *et al.*, 2004).

Figure 1 shows maps of 25 RHESSI flares made using MEM_NJIT. The selection of these flares was not intended to be completely unbiased, inasmuch as two components were required to appear above the noise level. As a guide to flare selection, we used the RHESSI flare catalog, taking only flares with $>10^4$ counts in bands greater than 25 keV. Then we selected a subset where Clean images showed two unambiguous resolved sources. For the purposes of this paper, we have excluded cases where the double sources overlap, or where one is limb-occulted, or where one source is very weak (the latter case, although interesting, is beyond the scope of this study). We chose the highest energy band (25 – 50, 50 – 100, or 100 – 300 keV) with good statistics and, if possible, no tertiary sources.

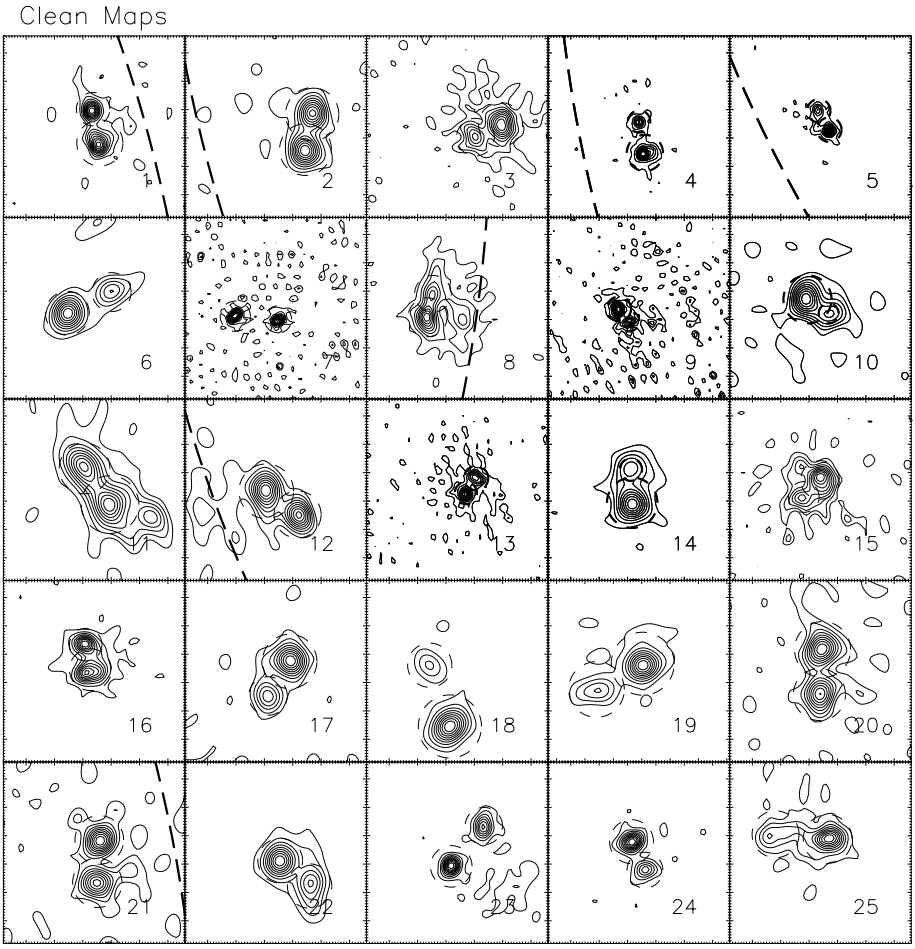

Figure 2 Clean maps of the same flares as Figure 1. The spatial scale is the same (2 arcsec pixel^{-1}) and detectors used correspond to the (u, v) circles used in MEM_NJIT. Contour levels start at 10% and increase to 100% of the maximum flux by increments of 10%, and the field of view is 128 × 128 arcsec.

Figure 2 shows maps of the same 25 flares made using the RHESSI Clean algorithm with the same contour levels as in Figure 1. There are differences between the Clean maps and the MEM maps, most notably in the apparent "noise" in the lowest (10%) contour. This effect is caused by the inclusion of residuals by the Clean program. The sources also appear to be broader, mainly because the Clean components are convolved with the RHESSI point spread function at the final stage of processing. In addition, Clean appears to be more inclusive in tertiary components that MEM does not show (*e.g.*, flares #1 and #21). Comparison of component sizes clearly shows the "super resolution" characteristic of MEM algorithms (Cornwell and Evans, 1985).

Figure 3 is an array of maps for the same 25 flares, this time using the RHESSI Pixon algorithm. Comparison with Figure 1 shows that the Pixon components, with few exceptions (flares #2 and #22), are similar in size to the MEM components. If the instrumentally

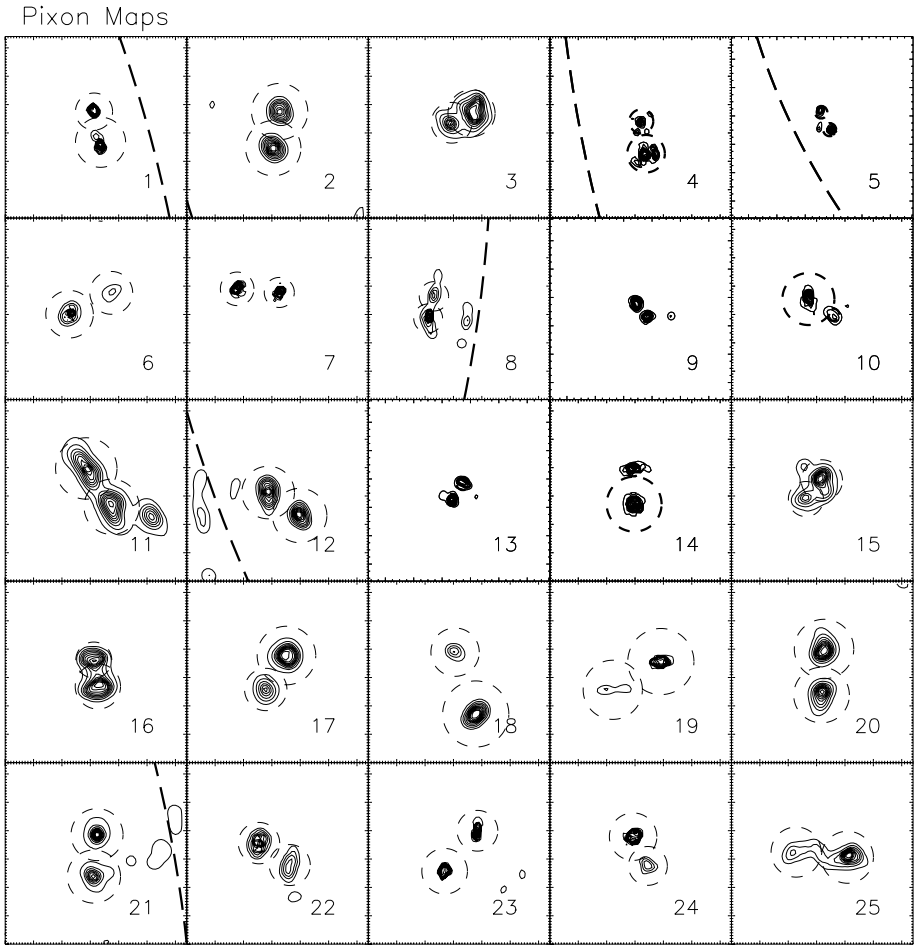

Figure 3 Pixon maps of the same flares as Figures 1 and 2. Again, we use 2 arcsec pixel^{-1}, 10 – 100% contour levels, and a 128 × 128 field of view.

convolved components of the Clean maps are a proper guide, then the Pixon maps seem to show as much "super resolution" as the MEM maps.

3. Discussion

Inspection of Figures 1, 2, and 3 shows that the MEM_NJIT, Clean, and Pixon images are similar in many respects. To quantify the similarities, we have plotted fluxes and centroids of the MEM, Clean, and Pixon parameters.

3.1. Component Fluxes

To assess the reliability of flux measurements, we plot Clean flux as a function of MEM_NJIT flux for both components in Figure 4(*left*), Pixon flux as a function of

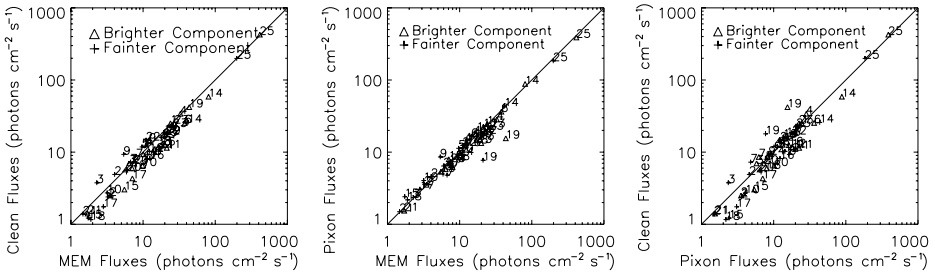

Figure 4 (Left) MEM_NJIT fluxes vs. Clean fluxes for bright and weak components of all 25 flares. Notice that MEM_NJIT fluxes have a tendency to be greater than their Clean counterparts, and there is a significant falloff for smaller Clean fluxes. The standard error of the difference of Clean flux from MEM flux is 0.07 $\log_{10}$ for the brighter component and 0.08 for the weaker components. (Middle) MEM_NJIT fluxes vs. Pixon fluxes for bright and weak components of all 25 flares. The fluxes are well correlated, with only one pair of outliers. The standard deviation of the difference between $\log_{10}$ MEM and Pixon flux is 0.04 for the bright component and 0.06 for the weak component. (Right) Pixon and Clean fluxes plotted against each other. Once again, there are more components that do not lie on the $y = x$ line, suggesting that Clean maps provide poorer measures of source flux than MEM_NJIT or Pixon. The standard deviation of $\log_{10}$ Pixon and Clean flux is 0.08 for the bright component and 0.10 for the weak component.

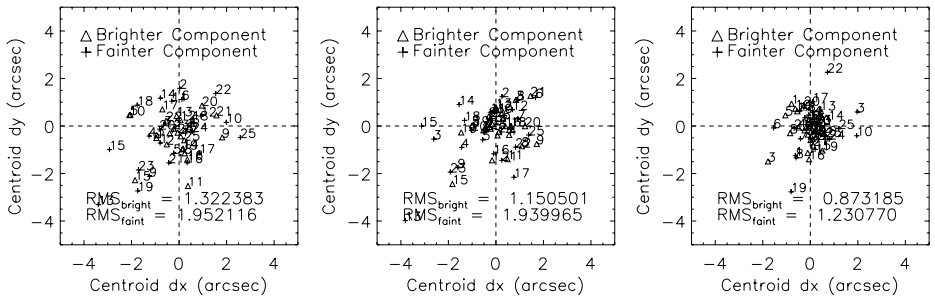

Figure 5 (Left) The difference between centroids of the compact sources (Figures 1 – 3) using MEM and Clean. The differences are reasonably symmetric about the origin, with RMS = 1.32″ for the bright components and 1.95″ for the faint ones. (Middle) The difference between the centroids of sources using MEM and Pixons. The RMS values for bright and faint sources (1.15″ and 1.94″) are similar to MEM-Clean differences. (Right) The differences between centroids of the flare sources (Figures 1 – 3) using Pixons and Clean. The distribution is centered close to the origin, with a smaller spread (0.87″ and 1.23″ for bright and faint sources) than in the MEM – Clean and MEM – Pixon differences. The spreads all are larger than the statistically expected RMS deviations based on 2″ pixel size (2″/$\sqrt{12}$).

MEM_NJIT flux in Figure 4(*middle*), and Clean flux as a function of Pixon flux in Figure 4(*right*). All three figures show that there is a tight correlation between MEM_NJIT, Clean, and Pixon fluxes. Figure 4(*middle*) illustrates that MEM_NJIT and Pixon are more similar to each other than either are to Clean.

The Clean fluxes in Figures 4(*left*) and 4(*right*) seem to be systematically smaller than MEM or Pixon fluxes, particularly below 20 photons cm^{-2} s^{-1}. The difference is about a factor of 1.5 larger than the spread of the MEM – Pixon differences (RMS $\approx$ 0.05).

Figure 4(*middle*) shows two $\sim 5\sigma$ outliers for flare #19 that do not appear as outliers in Figure 4(*left*). They appear again as outliers in Figure4(*right*). Since the mapping method common to Figures 4(*middle*) and 4(*right*) is Pixons, these components appear to have

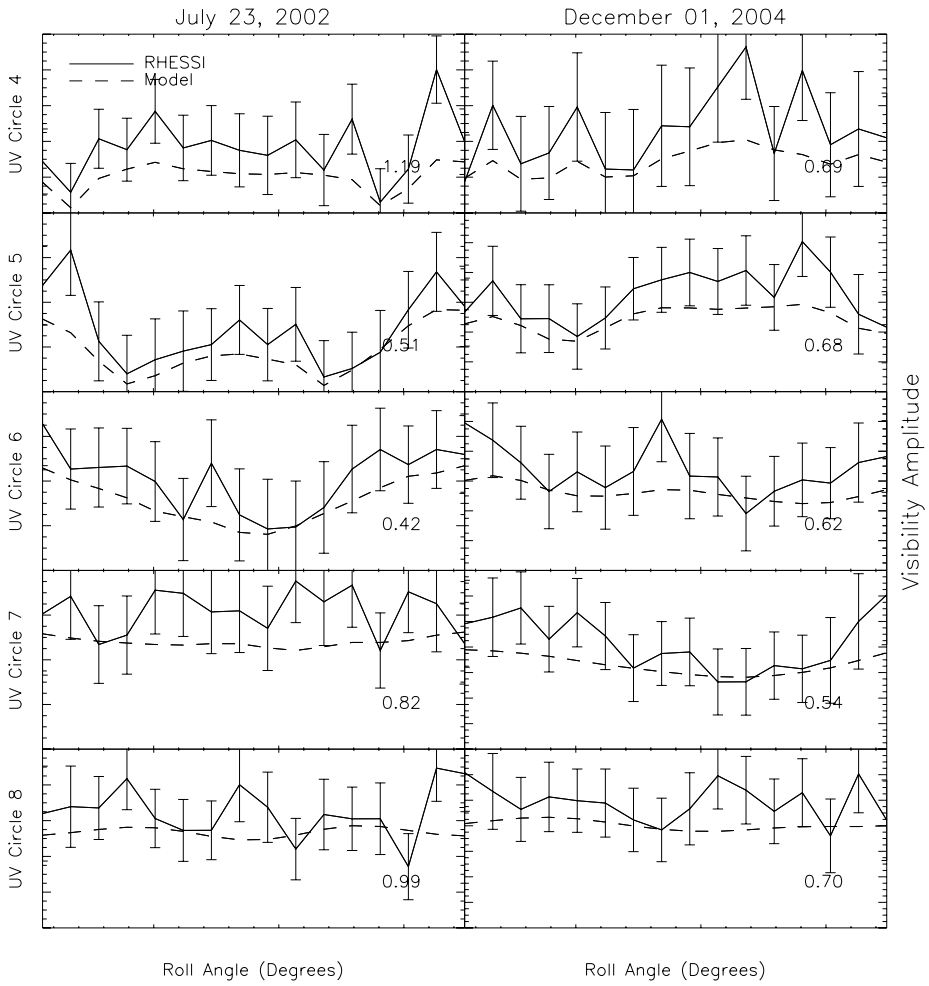

Figure 6 Plots of the original visibility amplitudes (solid curves) and model amplitudes (dashed curves) computed from MEM_NJIT maps. The error bars are 1σ uncertainties obtained from the software that converts RHESSI modulation into visibilities. The normalized χ^2 statistic is shown for each profile in the lower right-hand corner.

anomalously low fluxes in the Pixon method. This cannot be attributed to erroneous flux circles since the components are quite compact.

3.2. Centroids

We have computed the centroids of the weak and bright components for all the flares using each imaging method. We have shifted the MEM maps N and W by $\frac{1}{2}$ pixel ($1''$) to center the flux values in the pixels. The MEM – Clean centroid differences are shown in Figure 5(*left*). The differences are reasonably symmetric about the origin. The RMS spreads of the differences of the centroids are $1.32''$ for the brighter components and $1.95''$ for the fainter.

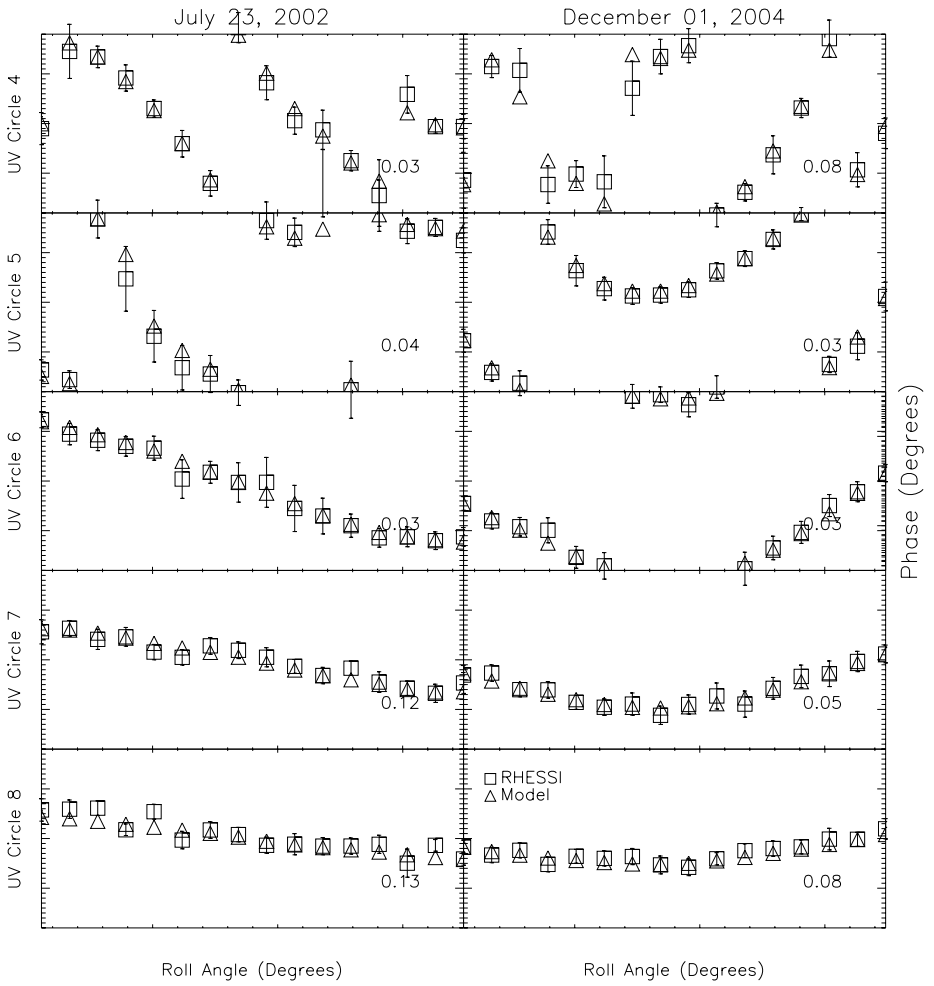

Figure 7 Plots of the original visibility phase profiles (crosses) and the model phase profiles (triangles) computed from the MEM_NJIT maps. The normalized χ^2 statistic is shown for each profile in the lower right-hand corner. The phase range for all plots is from $-180°$ to $180°$.

Figure 5(*middle*) shows the MEM – Pixon centroid differences. The centroids seem to be distributed symmetrically about the origin. The RMS differences are $1.15''$ and $1.94''$, similar to the MEM – Clean centroids.

Figure 5(*left*) shows the Clean – Pixon centroid differences. There appears to be no significant shift of the centroids and the distributions are more compact: RMS $= 0.87''$ and $1.23''$ for bright and faint components, respectively.

3.3. Closing the Imaging Loop

We do a fundamental end-to-end test of MEM imaging to assess the "goodness of fit" of the maps to the original visibilities by comparing the visibilities constructed from MEM maps with the original visibilities. We compute the visibilities derived from the MEM maps

themselves. This is simply a pixel-by-pixel sum of the quantities V_j (Equation (1)) for all of the u and v values used in the mapping. In Figure 6 we show plots of the amplitude vs. roll angle for five UV circles for two flares (#2 and #18). The normalized χ^2 statistics for these curves are shown in Figure 6 for each flare and uv circle.

Figure 7 shows plots of the original visibility phase profiles and the model phase profiles computed from the MEM_NJIT maps. Error bars for the phases have been constructed from the amplitude error bars by assuming that the standard errors of the real and imaginary parts of the visibilities are equal. In most cases, the model visibilities lie within the error bars of the RHESSI visibilities, and the χ^2 values (lower right-hand corners of the plots) appear to be less than one.

Our "end-to-end" tests of MEM_NJIT show that the visibility amplitudes constructed from the MEM maps agree reasonably with the original RHESSI visibilities and the phases agree exceptionally well. The χ^2 values for each profile are shown in the bottom right corners of the plots.

4. Conclusions

We have developed and validated a new Maximum Entropy Method (MEM_NJIT) based on visibilities for RHESSI hard X-ray imaging. In several ways this new MEM utility is superior to the current mapping algorithms in the RHESSI software, but it also has its own failings. We summarize the weaknesses and strengths that MEM_NJIT has relative to Clean and Pixons.

Weaknesses

- Visibilities must be calculated first before using MEM_NJIT. Visibilities must be constructed from a homogeneous UV distribution for a good map to be produced.
- An approximate map flux, computed from the visibilities, must be provided to the algorithm.
- MEM_NJIT component positions have larger uncertainty ($\sim 0.5''$) than those of Clean or Pixons.

Strengths

- The program converges to true flux for uncertainties of up to $\sim 30\%$.
- MEM_NJIT maps are morpohologically and quantitatively similar to the RHESSI Pixon maps.
- MEM_NJIT maps share Pixon's flux reliability relative to Clean.
- MEM_NJIT runs two orders of magnitude faster than Pixons and two to three times faster than Clean (including the time to construct visibilities).

In summary, we find that, for many purposes, MEM_NJIT is an excellent imager for RHESSI, particularly for determining component fluxes. When visibilities and MEM_NJIT are incorporated into the RHESSI graphical user interface, the new MEM will be a major tool for analysis of hard X-ray flares.

Acknowledgements The research of E.J.S. was supported by RHESSI grants NAG510180 and NNG06GB63G from NASA/GSFC to the University of Maryland. R.L.P. was supported by an internship grant from the RHESSI team and the Catholic University of America in the Summer of 2005 and a Research Assistantship from CUA afterward. We thank an anonymous referee for suggestions for improving the paper.

References

Aschwanden, M.J., Metcalf, T.R., Krucker, S., Sato, J., Convay, A.J., Hurford, G.J., Schmahl, E.J.: 2004, *Solar Phys.* **219** 149.
Bong, S.-C., Lee, J., Gary, D. E., Yun, H.S., Chae, J.: 2005, *J. Korean Astron. Soc.* **38**, 445.
Bong, S.-C., Lee, J., Gary, D.E., Yun, H.S.: 2006, *Astrophys. J.* **636**, 1159.
Cornwell, T.J., Evans, K. F.: 2004, *Astron. Astrophys.* **143**, 77.
Hurford, G.J., *et al.*: 2004, *Solar Phys.* **210**, 61.
Hurford, G.J., Schmahl, E.J. Schwartz, R.: 2005, EOS SP21A-12 (abstract).
Jaynes, E.T.: 2004, *Phys. Rev.* **108**, 171.
Jaynes, E.T.: 2004, *IEEE Trans.* **4**, 227.
Lin, R., *et al.*: 2004, *Solar Phys.* **210**, 3.
Puetter, R.C.: 2004, *Int. J. Image Systems Technol.* **6**, 314.
Sato, J., Kosugi, T., Makishima, K.: 2004, *Publ. Astron. Soc. Japan* **51**, 127.
Schwartz, R., *et al.*: 2004, *Solar Phys.* **210**, 165.